Proceedings of ASME Turbo Expo 2023
Turbomachinery Technical Conference and Exposition
GT2023
June 26-30, 2023, Boston, Massachusetts, USA

GT2023-102622

INVESTIGATIONS OF THE UNSTEADY SHOCK-BOUNDARY LAYER INTERACTION IN A TRANSONIC COMPRESSOR CASCADE

Edwin J. Munoz Lopez*
Alexander Hergt
Joachim Klinner
Sebastian Grund
Jirair Karboujian
Jasmin Flamm
German Aerospace Center (DLR)
Cologne, Germany

Volker Gümmer
Technical University of Munich (TUM)
Garching, Germany

ABSTRACT

The performance of compressor blades in transonic flow conditions is heavily hampered by unsteady flow effects caused by the Shock-Boundary Layer Interaction (SBLI). Even though these effects have been subject to research for a long period of time, very little is still known about the physical mechanisms driving the unsteadiness. In order to help elucidate the nature of these interactions in turbomachines, the recently designed Transonic Cascade TEAMAero was tested at the DLR's Transonic Cascade Wind Tunnel facility in Cologne. The cascade flow was measured with a unique high-speed Schlieren configuration capturing three adjacent passages simultaneously, along with unsteady total pressure measurements at the outlet, and unsteady acceleration measurements on the tunnel sidewalls. The results indicate that the main oscillation of the shocks is broadband at relatively low frequencies around 550 Hz for the aerodynamic design point, and 180 Hz for the off-design point. A further high-frequency tone is observed around 1140 Hz throughout. These frequencies were also observed with the different measurement devices employed. Cross-correlations between the signals indicate that there are different mechanisms at play between the passages that cause both upstream and downstream transmission of information. Because of this, the shock oscillations were not always in-phase between adjacent passages. The results help characterize the SBLI behavior of the cascade in the wind tunnel, aiding future numerical and experimental efforts aiming to decipher the inherent mechanisms causing it.

Keywords: Compressors, SBLI, Experimental, Unsteady, Schlieren

*Corresponding author: edwin.munozlopez@dlr.de

NOMENCLATURE

Acronyms

ADP	Aerodynamic Design Point
DC	DownCenter
DO	DownOff
DW	DownWake
HSS	High-Speed Schlieren
L2F	Laser-2-Focus
MP	Measurement Plane
ODP	Off-Design Point
PCB	PicoCoulomB acceleration sensor
SBLI	Shock-Boundary Layer Interaction
TCTA	Transonic Cascade TEAMAero
TGK	Transonic Cascade Wind Tunnel
UC	UpCenter
UW	UpWake

Latin letters

$AVDR$	Axial velocity density ratio = $\rho_2 V_2 \sin\beta_2 / \rho_1 V_1 \sin\beta_1$
c	Blade chord [mm]
FT	Flow turning = $\beta_1 - \beta_2$ [°]
M	Mach number
P	Power [W]
p_t	Total pressure [Pa]
WR	Working range [°]
x_s	Shock position [mm]

Greek letters

β	Flow or geometry angle [°]
ω	Total pressure loss coefficient = $(P_{01} - P_{02})/(P_{01} - P_1)$

Superscripts and subscripts

1	Inlet value
2	Outlet value

1. INTRODUCTION

The presence of Shock-Boundary Layer Interaction (SBLI) on airfoils has been noted and studied for over 70 years now, as commented by Dolling in [1]. In spite of this, very little is still understood about the physical mechanisms driving this phenomenon that is ubiquitous to high-speed flow applications. The literature for instance counts with a diversity of theories with very different concepts. Many of these supported by independent experimental or high-fidelity CFD verifying one or the other, sometimes in a contradicting manner. However, despite this extensive amount of work and diversity of thought, not much can still be said on what makes one mechanism more prevalent than another for a given design or application. This in turn means that little can be done to predict this behavior, and even less to mitigate it.

The most recognizable theories on non-aeroelastic interactions can be briefly described as follows: Lee's soundwave feedback mechanism describing disturbances produced by the shock that interact with the trailing edge to generate soundwaves that travel upstream on the suction side [2, 3]; or disturbances that travel along the pressure side and around the leading edge to arrive again to the shock [4]; or disturbances that are generated downstream of the shock and travel upstream directly affecting the incoming boundary layer as described recently in [5, 6]. These in addition to the mechanisms suggested in fundamental studies of oblique shocks with basic geometries, which suggest that the interaction of the shock with its own separation bubble can also lead to low-frequency oscillations that are sometimes within the ranges observed for the aforementioned applications [7, 8]. Many of these are supported by observations in high-fidelity CFD investigations such as [9–11] to name and cite a few.

Within the context of engine compressors, the necessity to understand these mechanisms and mitigate this behavior cannot be understated. This was highlighted by Hergt in [12] on a modern 2D design, where it was shown how the stability, reliability, and operability of any such component is negatively affected. This behavior has also been observed in [13, 14] to cause additional loss mechanisms in 3D rotor configurations. However, in order to be able to understand and mitigate such phenomenon, Dolling points out that a larger set of high-quality unsteady experimental data is first required. Such studies would then be able to support theoretical models and high-fidelity CFD investigations to start deciphering the complex phenomena at play [1]. This has been the work envelope picked up by the research community in the form of international collaborations and thorough experimental investigations, as observed in [15–18] among others.

The DLR has also been an active player on this front thanks to the Transonic Cascade Wind Tunnel (TGK) available in Cologne. This facility has been developed for over 40 years now for the purpose of transonic compressor cascade testing, allowing notable contributions to the field on how to design, operate, and report on such investigations [19–21]. The TGK's linear cascade and continuous loop configuration, with variable inlet Mach Number up to 1.4 and Reynolds numbers between 10^5 and $3 \cdot 10^6$, allows for both great operability and enviable optical access to study the aforementioned flow behaviors. In addition to this, new measurement techniques have been developed for the wind-tunnel in recent years, which have allowed the publication of high-quality unsteady experimental data focused on the phenomena of interest. This includes one-of-a-kind PIV, High-Speed Schlieren (HSS), and High-Speed PIV measurements of different modern cascade profiles that help address some of the shortcomings in the literature noted by Dolling [5, 6, 12].

The focus of this paper is then to build on this line of work at the DLR's Institute of Propulsion Technology by combining a number of unsteady measurement techniques in order to extract new information on the mechanisms of SBLI inside a wind tunnel for a new compressor cascade design. This is done with simultaneous HSS recordings of multiple passages in the cascade, along with Kulite pressure measurements in the wake, and piezoelectric (PCB) acceleration measurements at different positions in the wind tunnel. The paper then begins by introducing the Transonic Cascade TEAMAero (TCTA), which is the product of a recent optimization work performed by the author in [22, 23] under the ongoing research consortium, TEAMAero [24]. This is continued by a thorough overview of the experimental facilities and unsteady measurement equipment employed. The results obtained from the measurement campaign are then presented with a thorough discussion of the phenomena observed; before giving some of the author's concluding perspectives on these unique measurements for the wide-reaching research effort on SBLI flows.

2. THE TRANSONIC CASCADE TEAMAERO

The cascade used for this study is the Transonic Cascade TEAMAero, or TCTA. This cascade is derived from the optimization work performed by the author in [22] through the use of advanced in-house numerical methods including the optimization suite, *AutoOpti*, coupled with the CFD solver for turbomachinery applications, *TRACE* [25, 26]. The objective of this multi-objective optimization was to provide a new cascade design that was representative of a transonic section from a modern compressor rotor. This was achieved thanks to the following features: a considerable set of 21 degrees of freedom to define the 2D shape; a thoughtful design space and CFD strategy based on previous experience at the institute; and the use of two main objective functions set to minimize the losses at the design point and over the working range. Starting from these results, the original design obtained was adapted for the purpose of the experimental campaign and its performance was validated. These topics will be briefly described in the following sections.

2.1 Cascade Design Overview

Starting from the result in [22] for the *best* cascade from the optimization, its design was modified slightly in order to aid its manufacturability and operability for the purpose of the experimental campaign. The design of the TCTA was then obtained by increasing the ratio between the leading edge length and its radius, and decreasing the pitch of the cascade to reduce the mass flow load on the wind tunnel. The parameters modified were however always maintained within the optimization's design space in order

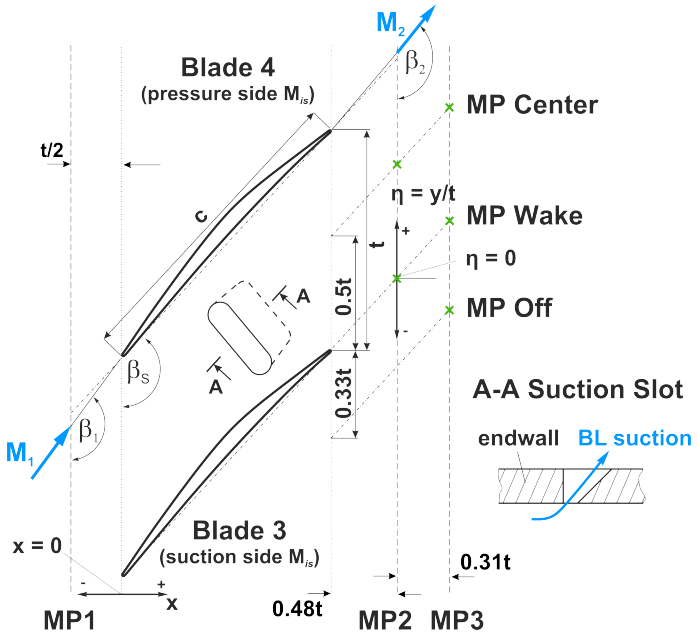

FIGURE 1: TCTA CASCADE DESIGN AND CONFIGURATION

to ensure that the final design was comparable and representative of the optimization strategy followed.

The final design of the TCTA along with the cascade configuration used for the campaign is shown in Fig. 1. In this figure, the different geometrical definitions of the cascade are shown, along with the design of the sidewall suction slots based on previous testing experience at the TGK and that are located at 80% of the blade chord [12]. These slots help control the size of the sidewall boundary layer during the experiments, and therefore the operating point of the cascade. The cascade is instrumented with five pressure taps per cascade pitch at the inlet and outlet Measurement Planes (MP) 1 and 2 shown in the figure. The cascade also counts with pressure taps on the suction and pressure sides of the 3rd and 4th blades, respectively. The different general cascade properties of interest are then summarized in Tab. 1.

2.2 Validated Cascade Performance

The performance of the cascade has been validated in a previous experimental campaign. This campaign was focused on steady measurements, where the inlet flow angle at the MP1 was additionally measured with a laser anemometry technique, Laser-2-Focus (L2F) [12, 27], and the outlet flow was captured with traverses of a three-hole probe at the MP2. The measurements were averaged to a uniform flow far downstream of the cascade based on the conservation equations, as explained in [21], in order to report on the overall performance of the cascade. This performance was primarily measured based on the total pressure loss coefficient (ω), the flow turning (FT), and the Axial Velocity Density Ratio ($AVDR$). The latter being a parameter that indicates the amount of area contraction in the passage of the cascade due to the presence of the sidewall boundary layer [20].

The results indicated that the cascade preferably operates in the wind tunnel at its design inlet Mach number at an $AVDR$ of 1.05. The performance of the cascade was then validated near the design inlet flow angle to define the Aerodynamic Design Point (ADP) for the campaign. In addition to this, a further operating point was investigated that would provide perspective and a point of comparison on the unsteady SBLI behavior of the cascade under different operating conditions. This point was defined as the Off-Design Point (ODP), obtained at a lower inlet Mach number of 1.04, but operating at similar inlet flow angle. These operating points are summarized in Tab. 1. Additionally, the respective isentropic Mach number (M_{is}) distributions measured for these operating points are shown in Fig. 2, along with the calculated CFD-RANS distributions used as reference.

TABLE 1: TCTA DESIGN PROPERTIES AND OPERATING POINTS.

General	
Total blade count	6
Blade chord (c)	100 mm
Cascade pitch (t)	65 mm
Stagger angle (β_{st})	135.8°
Working Range (WR)	>2°
Aerodynamic Design Point (ADP)	
Inlet angle (β_1)	146.4°
Inlet Mach number (M_1)	1.22
Reynolds number	$1.35{\cdot}10^6$
$AVDR$	1.05
Losses (ω)	0.1205
Flow turning (FT)	10.1°
Off-Design Point (ODP)	
Inlet angle (β_1)	146.1°
Inlet Mach number (M_1)	1.04
Reynolds number	$1.315{\cdot}10^6$
$AVDR$	1.16
Losses (ω)	0.0665
Flow turning (FT)	13.8°

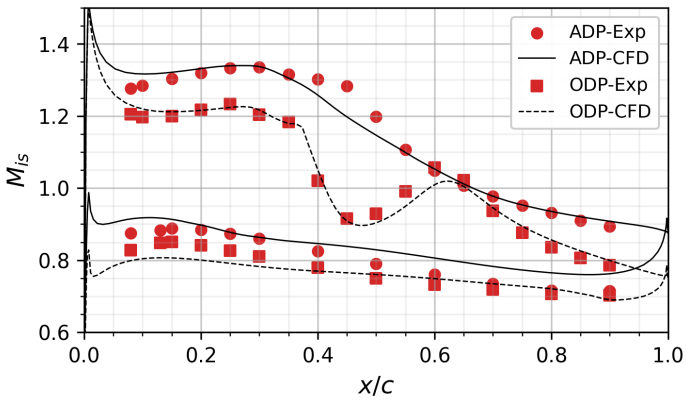

FIGURE 2: ISENTROPIC MACH NUMBER DISTRIBUTIONS OF THE TCTA CASCADE AT THE ADP AND ODP.

3. EXPERIMENTAL METHODS

In order to address the goal of this paper, considerable effort went into preparing the new measurement techniques that would

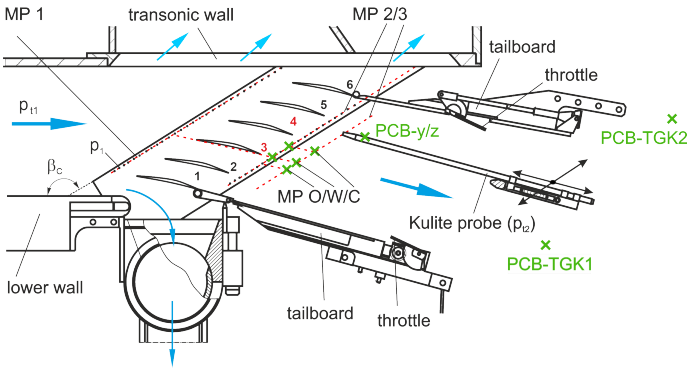

FIGURE 3: TGK FACILITY CONFIGURATION WITH THE TCTA

allow new and unique insights into the unsteady SBLI properties of the TCTA. These items are presented in this section, starting with a description of the TGK facility itself, before proceeding with a rundown of the steady, and unsteady measurement techniques employed throughout the investigation.

3.1 The Transonic Cascade Wind Tunnel

As mentioned in Section 1, the TGK is a state-of-the-art facility for the study of compressor cascade flows, developed over a long time to operate in difficult transonic flow conditions. The TCTA is first mounted on plexiglass sidewalls and then inside the TGK's test section as shown in Fig. 3. This figure also presents the following main features offered by the TGK to conduct this type of experiments: a) good optical access to the flow going through the cascade; b) a variety of control surfaces and suction devices that can be operated throughout the experiment to adjust the operating point, such as the upper and lower tailboards and throttles, and the suction devices after the lower wall and over the upper transonic wall; c) the possibility to rotate the test section to a desired cascade angle (β_C), which for this campaign was maintained at 147°; and d) the availability of a probe at the outlet, which can be operated to different positions of interest.

3.2 Steady Measurement Techniques

The operating points of the cascade were confirmed in separate test runs before and after the unsteady measurement tests. These points would then be measured with the different techniques already mentioned in Section 2, including the pressure taps installed, the L2F angle measurements, and the three-hole probe traverses over MP2. Schlieren images of the shock structure for each operating point were also captured with a CMOS video camera at 21 fps, as shown in Fig. 4. For the unsteady measurement tests on the other hand, the three-hole probe was changed for an unsteady Kulite total pressure probe. Because of this, the operating point was searched by matching the previously gathered inlet flow Mach number distribution and the isentropic Mach number distribution through the middle passage.

3.3 Unsteady Measurement Techniques

This experimental campaign focused on implementing a host of unsteady measurement techniques at different locations in the test area in order to gather unique information of the SBLI behavior inside a transonic cascade. This was done with simultaneous

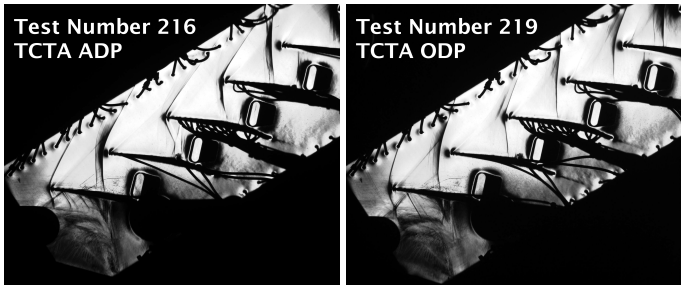

FIGURE 4: TCTA SCHLIEREN CAPTURES FOR THE ADP (LEFT), AND ODP (RIGHT).

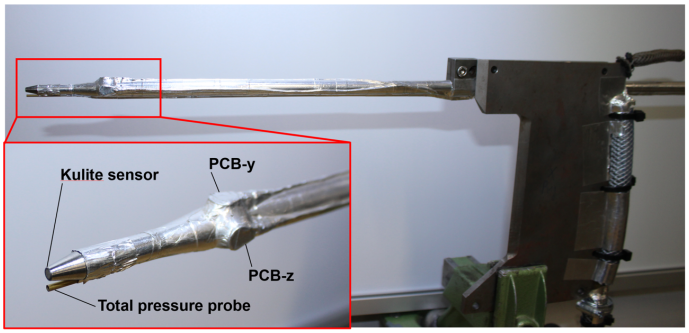

FIGURE 5: CUSTOM PROBE FITTED WITH KULITE AND PCB ACCELERATION SENSORS.

unsteady measurements with a new total pressure Kulite probe, a new set of PCB sensors, and a unique High-Speed Schlieren (HSS) configuration as described in the following sections.

3.3.1 Kulite Probe and Acceleration Sensors. For the unsteady measurement tests, the three-hole probe was substituted with a custom Kulite probe to capture time-accurate measurements of the outlet flow's total pressure. The Kulite sensor of model XCS-093-D with "M"-type screen was mounted directly at the front of the probe, as shown in Fig. 5. This configuration helps avoid additional Helmholtz-type resonance issues than those of the sensor itself, which has a flat frequency response up to 21.5 kHz [28]. In addition to the Kulite, two more unsteady signals were captured with the probe from PCB sensors 50 mm downstream. These sensors were attached to the probe's shaft and oriented to capture the movement of the probe in its local y and z-directions, or in the direction perpendicular to the blade chord and towards the wind tunnel's sidewalls, respectively.

The probe was used to perform measurements at five locations corresponding to the intersections between the MPs 2 and 3 with the MPs Off, Wake, and Center. Note that the MPs 2 and 3 will also be referred to as MPs Up and Down for upstream and downstream, respectively. In total, there were five measurement points, which are marked with a green "X" in Fig. 1. Lastly, the approximate locations of the measurement planes with the probe and the PCB-y and PCB-z sensors are sketched in Fig. 3.

In addition to the probe, two more PCB sensors were also installed on the wind tunnel itself. The first sensor, PCB-TGK1, was installed on the outer side of the sidewall approximately 590 mm downstream of the MP2 along the chord axis of the 2nd blade.

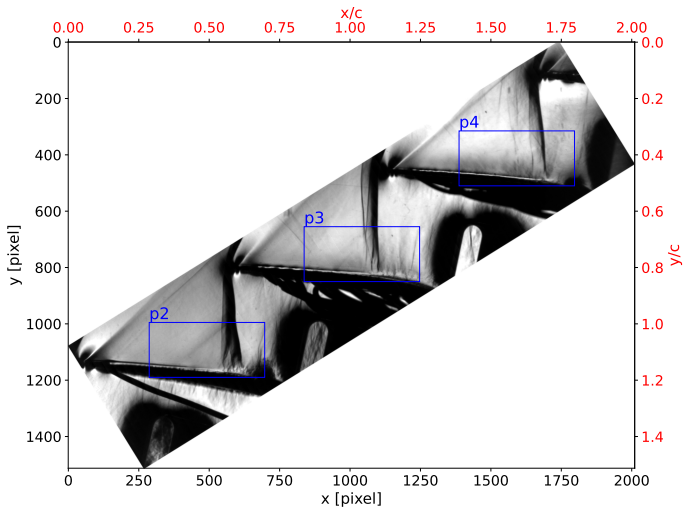

FIGURE 6: HIGH-SPEED SCHLIEREN SAMPLE IMAGE WITH REGIONS USED FOR SHOCK DETECTION.

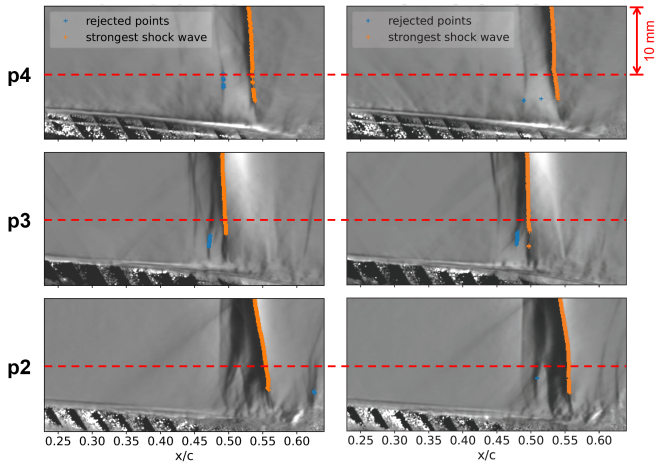

FIGURE 7: TWO PROCESSED CONSECUTIVE SCHLIEREN SNAPSHOTS (LEFT AND RIGHT) OF 50 µs TIME SEPARATION, WITH THE PASSAGE SHOCK DETECTED IN FOCUS REGIONS PER FIG. 6.

The second and final sensor, PCB-TGK2, was installed inside the wind tunnel, but far downstream on one of the surfaces that deviates the flow towards the rest of the tunnel circuit. This sensor is located approximately 700 mm from the upper tailboard in the horizontal direction. Both of these sensors are oriented in the same direction as the probe's PCB-z sensor, and their approximate locations are marked in Fig. 3. Finally, the data acquisition system used for all the aforementioned devices was the TRION-2402-MULTI universal analog module. The sampling rate for all the measurements was 200 kHz and the expected accuracy of the signal corresponds to 0.02% of the analog reading. Note that the acceleration signal from the PCB sensors was typically integrated into velocity readings directly by the data acquisition system.

3.3.2 High-Speed Schlieren Imaging and Processing.

The HSS imaging is based on a conventional z-configuration that includes a 4 mm wide slit and a cut-off edge, both oriented approximately perpendicular to the inflow direction to maximize image contrast of the passage shocks. For high-speed recording, the field of view is 2048×512 pixels corresponding to 204.8×51.2 mm^2, or 10 pixel/mm, with the long side aligned parallel with the leading edges of the blades and extending downstream to the boundary layer suction slits (see Fig. 6). At the given image size, the camera (i-speed 7, IX cameras) can maintain frame rates of 20 kHz which was considered sufficient to track the passage shocks, which move at maximum velocities of O(10 m/s) for the given operation conditions [6].

The illumination is provided by a pulsed green HP-LED [29, 30]. To minimize blurring of the moving density gradients, the LED (OSRAM LE CG P2A) is operated at an effective pulse width of 1 µs using a modified high-current driver, which reduces the slow rise time of O(500 ns) of the LED's emission to approximately 170 ns [31]. In order to optimize the operating conditions and periodicity of the cascade flow prior to high-speed imaging, the beam is redirected by a retractable mirror to the CMOS video camera observing the entire shock system as shown in Fig. 4.

At each unsteady measurement position described, two bursts of 0.482 s duration were captured containing 9639 images each. Prior to the automatic detection of the shock positions in the passages, contrast enhancement is performed by normalization with the average image of each burst. Each image is then rotated using bi-linear interpolation so that each image row is aligned parallel with the inflow direction of the transonic nozzle. This is done while maintaining the image scale at mid-span (10 pixel/mm). The passage shocks are then tracked in three regions of 410×195 pixels (41.0×19.5 mm^2) as indicated in Fig. 6. These regions start at the 22.6% blade chord point. Care was taken to ensure that the range of shock excursions is covered by these regions based on the intensity minima of each burst.

To detect the position of the passage shock, candidates are first searched based on the maximum of the discrete intensity difference evaluated in each image row. To reject outliers and to find connected x-positions on the strongest gradient along image rows (transverse direction), the median is determined and the larger number of points above or below the median is retained. Both steps are repeated until the largest difference between the valid x positions is below a certain threshold (0.5 mm). Detected passage shocks including valid and rejected positions are shown in Fig. 7 for two consecutive images of the three passages.

For the purpose of further analysis and comparison with the rest of the unsteady measurement sensors, the x_s positions were averaged row-wise within a 10 mm region from the top, as shown in Fig. 7. This helps avoid the regions closer to the blade, where the normal shock occasionally splits into a lambda pattern. Furthermore, in order to synchronize these sets of unsteady data, both the start and first frame-synchronization triggers of each of the bursts were additionally recorded by the data acquisition system at 200 kHz sampling. Finally, to allow cross-correlations between the unsteady data captured at different sampling frequencies, 20 kHz for the shock traces and 200 kHz for the remaining sensors, the latter recordings were low-pass filtered at a cut-off of 40 kHz and then downsampled to 20 kHz through linear interpolation, providing a common time base for analysis.

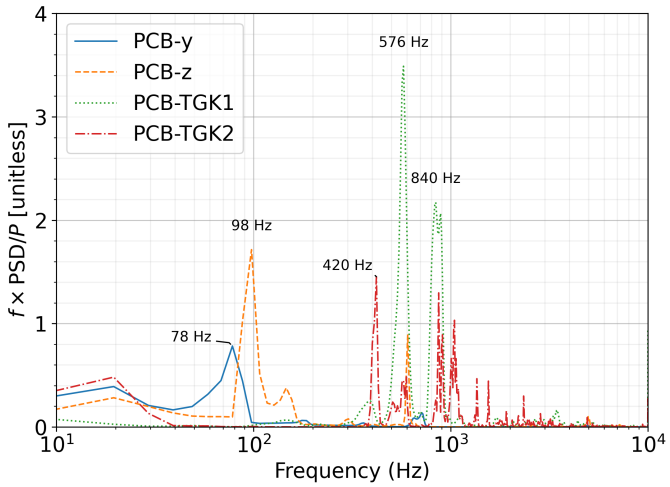

FIGURE 8: FREQUENCY WEIGHTED SPECTRA OF THE PCB SENSORS WITH SINGLE EXCITATION AND NO FLOW.

4. RESULTS AND DISCUSSION

The results for this experimental campaign were captured over the course of seven measurement days, many times preceded by weeks of preparation and planning. The measurement points are identified with a test number, as well as the location of the probe based on the relevant MPs, i.e. UpWake (UW), UpCenter (UC), DownWake (DW), DownCenter (DC), and DownOff (DO). The results are then presented in this section, starting with the modal analyses of the PCB locations performed without airflow in the wind tunnel, moving on to the analyses of the measurements at the cascade's ADP and ODP with signal spectra, and cross-correlations between the most relevant datasets.

4.1 PCB Sensor Modal Analyses without Flow

In order to capture the natural frequencies at the locations where the PCB sensors were installed, two tests were performed per sensor to measure the response to single impulse excitations without airflow. These impulses were provoked by hitting the component in question two times within a certain time interval near the location of the sensor. The tests were performed with all the components installed as they would be during the unsteady measurements with airflow. Regarding the spectra reported throughout the results section, the power scaling of the frequency weighted-spectrum is preferred, as the frequencies that are driving the power of the signal become much more evident than with the usual y-axis log scaling. This becomes particularly useful in latter sections when analyzing the frequencies of the shock movement [9]. Note that the parameter on the y-axis is normalized by the total integrated power (P) of each signal.

With this in mind, the frequency-weighted spectra obtained for each PCB sensor were averaged and are shown in Fig. 8, along with annotations of the dominant frequencies observed throughout. The figure shows that the components vibrate at predominantly lower frequencies under 1 kHz. This is especially the case with the probe, although being itself attached to the sidewall, it was also expected to show similar frequencies as the TGK1 sensor during the test with airflow. The sidewall itself clearly vibrates at a frequency band between 500 and 600 Hz, with a narrow peak at 576 Hz, in addition to a broader frequency band between 800 and 900 Hz. It will be later observed, that the frequencies of the sidewall become relevant during the analysis of the shock position. Finally, the deflecting surface on which the TGK2 sensor is installed shows multiple peaks across a wide range of frequencies, some of them shared with the TGK1 sensor.

4.2 ADP: Analysis of the Unsteady Measurements

At the cascade's ADP, two unsteady measurement recordings were made per measurement position shown in Fig. 1. A 50 ms sample trace of one such recording at the UpWake position is shown in Fig. 9. The top subfigure shows the trace of the shock position (x_s) in all the passages, with the origin and axes based on the shock detection regions shown in Fig. 6. There, it can be observed that the shock detection procedure is robust, albeit not perfect given that some "jumps" can be observed in the x_s signal, especially with the signal from the 4$^{\text{th}}$ passage (P4). Note that the signal has been passed through a median filter, and that the average error of the shock position throughout the measurement campaign was always estimated to be within 0.2 and 0.3 mm.

The few jumps that can still be observed are due to persistent offsets on the shock signal due to the integrated nature of the 2D image provided by the HSS system for what will always be a complex 3D shock front, as observed in Fig. 7. Additionally, this issue is thought to be intensified in the 4$^{\text{th}}$ passage due to the influence from the top cascade passage, which seemed to have a high amount of interaction with the upper wall due to the angle of the cascade with respect to the horizontal. This is nevertheless not expected to be a problem during analysis due to the robustness of the numerical methods employed and the length of the recordings. The bottom subfigure on the other hand shows the resampled signals captured directly and simultaneously by the Kulite and PCB-TGK1 sensors. In order to avoid cluttering, the other PCB sensors were not included, but the TGK1 sensor is representative of the measurements captured with the PCBs.

4.2.1 ADP: General Remarks on the Measurements.

The movement of the shock was observed to be fairly consistent between recordings, measurement positions, and the expectations given previous CFD-RANS simulations and previous testing experience. The average shock positions along the chord, x_s/c, for the 2$^{\text{nd}}$, 3$^{\text{rd}}$, and 4$^{\text{th}}$ passages were 55.4%, 53.7%, and 49.4%, respectively. These positions are reported with an estimated average shock detection error of 0.25% chord length and signal RMS values between 1.5% and 4%, with the lower values corresponding to the 3$^{\text{rd}}$ passage and the higher ones to the 4$^{\text{th}}$ passage. A similar observation can then be made with the maximum range of the shock excursions, which for the middle passage average to 11.8% chord length, while the upper passage reaches an average of 22.3%. As previously noted, even though the periodicity achieved at this operating point was good, it is clear from the behavior of the shock itself that the cascade operated with more unsteadiness and a slightly lower Mach number over the upper passages due to the interaction with the upper wall.

Regarding the other signals, statistics regarding the amplitude of the oscillations are a bit more difficult to interpret. The Kulite for instance will be ignored due to calibration problems

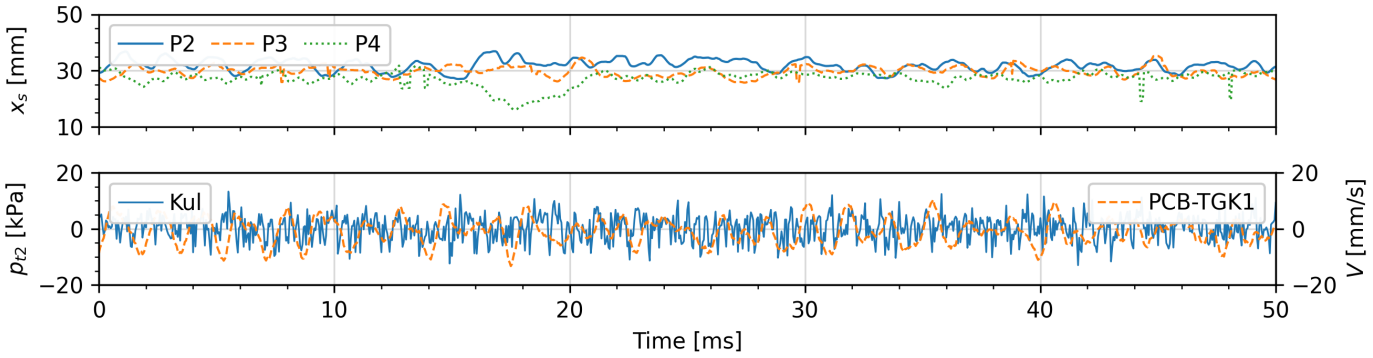

FIGURE 9: SAMPLE TIME TRACE OF SIMULTANEOUS RECORDINGS OF THE SHOCK POSITION x_s IN THE THREE PASSAGES (TOP), AND THE KULITE PROBE SENSOR AND PCB-TGK1 SENSOR (BOTTOM) AT THE ADP.

that have not been corrected on all the recordings. The PCBs on the other hand can be easily compared with each other, showing as expected that the probe vibrates more intensely than the heavier wind tunnel components; about one order of magnitude higher in terms of the velocity signal RMS value. When these velocity signals are integrated, the components are estimated to be vibrating at low amplitude ranges from approximately 0.2 mm for the wind tunnel sidewall and up to approximately 1 mm for the y-axis of the unsteady probe.

4.2.2 ADP: Signal Spectra Analysis. The unsteady characteristics of the shock position signals are now analyzed in more detail with the help of the frequency-weighted spectra in Fig. 10. The spectrum for each line is calculated from the average of the two different recordings taken. From the figures, it is evident that throughout the different measurement positions, the shock is predominantly moving at a lower broadband frequency range that peaks between 500 and 600 Hz. The only exceptions being the 4th passage spectra (top subfigure), which seems to show noisy broadband content at frequencies about an order of magnitude lower, possibly due to the aforementioned issues.

In addition to this lower frequency content, there is a clear peak in most spectra at a specific tone of 1143 Hz. This tone seems to be modulating the lower-frequency oscillations of the shock, based on observations of the signal traces such as Fig. 9. This tone is also very similar to one observed during a previous experimental campaign performed at the TGK with a different cascade design [12]. Even though the airfoil designs are considerably different, the cascades themselves have a lot of similar properties and operating conditions, such as chord, M_1, β_{st}, β_1, etc. This may suggest that this high frequency tone is generated through the interaction of the flow with these properties of the cascade, and/or with the wind tunnel itself. The exact origin of such a specific and persistent tone throughout the spectra is however difficult to estimate and will have to be looked at in detail in future studies. As a last point regarding the spectra, and using the DownOff position as a control case given that the probe was located away from the middle passage, the shocks are shown to behave consistently across the different probe positions.

The spectra of the Kulite, and the PCB-y and TGK1 sensors are then shown in Fig. 11 for the UpWake and UpCenter probe positions. The PCB-z and TGK2 sensors are left out given that

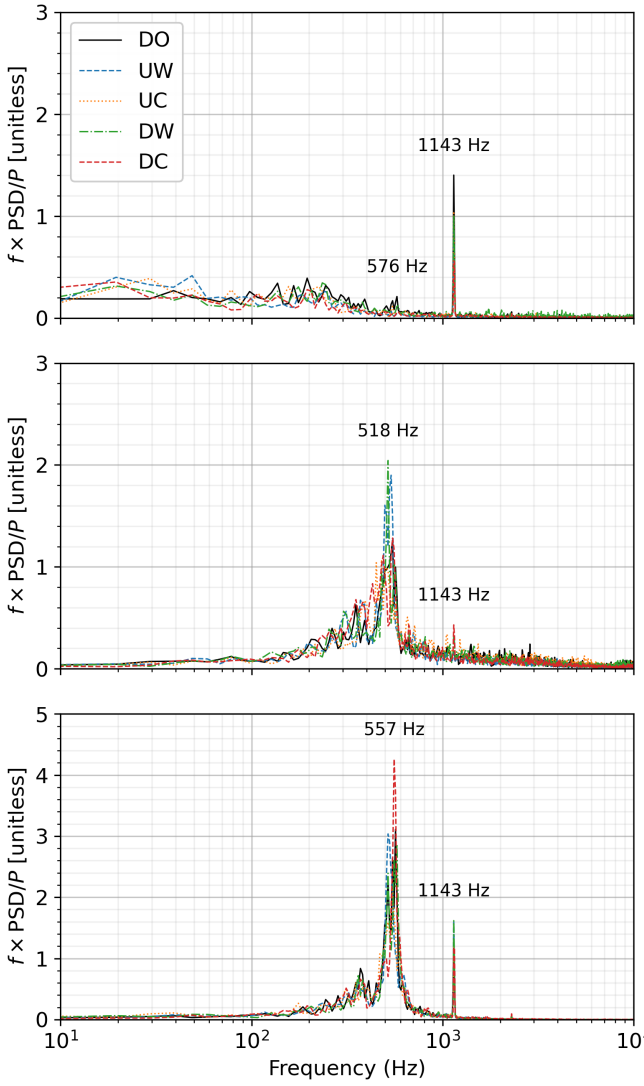

FIGURE 10: SHOCK POSITION SIGNAL SPECTRA FOR THE 4th, 3rd, AND 2nd PASSAGES (TOP TO BOTTOM) OVER DIFFERENT PROBE POSITIONS AT THE CASCADE'S ADP.

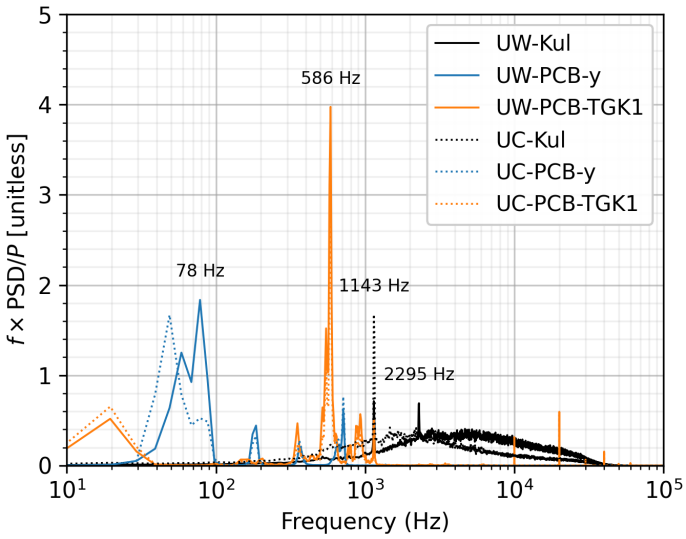

FIGURE 11: KULITE AND PCB SENSORS SIGNAL SPECTRA FOR THE UPWAKE, AND UPCENTER PROBE POSITIONS AT THE CASCADE'S ADP.

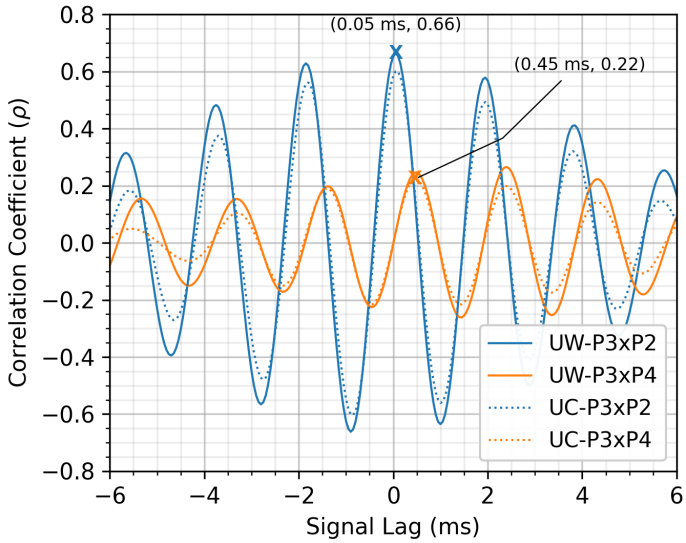

FIGURE 12: SHOCK POSITION SIGNAL CORRELATIONS BETWEEN THE CASCADE PASSAGES FOR THE UPWAKE AND UPCENTER POSITIONS.

they do not provide a lot of new information to the analysis. The spectra for all the components were nevertheless very similar to the modal frequencies shown in Fig. 8. The only exception was the PCB-z sensor, which proved to be influenced by the movement of the sidewall to which it is attached due to a similar dominant frequency peak near 600 Hz. Additionally, only the UpWake and UpCenter measurements are shown given that these transversal planes seemed to induce the biggest change on the spectra. That is to say, the UpWake and DownWake spectra were very similar to each other, while the same was the case with the UpCenter, DownCenter, and DownOff spectra. The latter being close to the same position along the 2nd instead of the 3rd passage.

From the figure, it is clear that the sidewall is moving primarily with a frequency band between 500 and 600 Hz, but peaking very narrowly at 586 Hz. The 840 Hz frequency shown in the modal spectra is still present, but to a much lower level in comparison, while the 1143 Hz tone is also present on the sidewall. This topology has some similarities with the shock spectra previously shown, although these would peak slightly earlier between 510 and 550 Hz, and they also presented some lower frequency content down to even 200 Hz. The PCB-y signal shows that the probes primarily vibrated at their lower modal frequencies, seemingly unrelated to the other signals in the analysis, except for some frequencies that seem to be still be shared with the sidewall.

The Kulite on the other hand is difficult to interpret, given that the spectra show a lot of broadband content across a whole decade or more. It is however noteworthy that these spectra don't show a peak around 500 Hz, when the tone at 1143 Hz is still clear along with what seems to be its harmonic at 2295 Hz. This could indicate either that the disturbances on the total pressure due to the shock motion are damped disproportionately at lower frequencies as the airflow travels downstream; or that these disturbances are generated somewhere else in the wind tunnel and travel in both directions with ease, given that they were observed in most of the spectra analyzed. As a last observation, the Kulite spectra are the ones that showed the biggest differences between Wake and Center planes. This is noted from the higher amplitude and power content at higher frequencies for the spectrum in the Wake position, which can be expected from a greater presence of turbulent structures coming from the wake of the blade itself.

The results at the ADP then seem to indicate that the HSS visualizations and the measurement sensors are seeing many of the same frequencies. This is especially the case with the lower frequency band, which is notably shared with the tunnel sidewall, but not with the Kulite. The higher frequency tone instead is seen in just about every relevant measurement sensor. This despite its narrow frequency range, including power and amplitude values that are smaller than the ones observed in the lower frequency band. The fact that the different measurements show some similar frequencies however provides little indication on where the disturbances actually originate, at the cascade or from the configuration of the wind tunnel. Some insights on this could be provided by correlating the signals, as is attempted in the following section.

4.2.3 ADP: Signal Correlations. The easiest set of correlations established is that between the shock position signals in the different passages, as shown in Fig. 12. In this figure, the signal from the 3rd passage has been used as the reference to correlate it with the signals from the 2nd and 4th passages. The lines are the result of the average between the correlations calculated for each recording. Additionally, given that the correlations of the full signal are difficult to interpret, the signals have been bypass filtered between 400 and 700 Hz to capture the frequencies of interest. Lastly, only the correlations from the UpWake and UpCenter planes are shown, though these can be considered representative of what was observed in the remaining locations.

Moving on to the results themselves, the correlations between the 3rd and 2nd passages showed consistently a peak correlation at a positive lag of 0.05 ms. This positive lag indicates that there

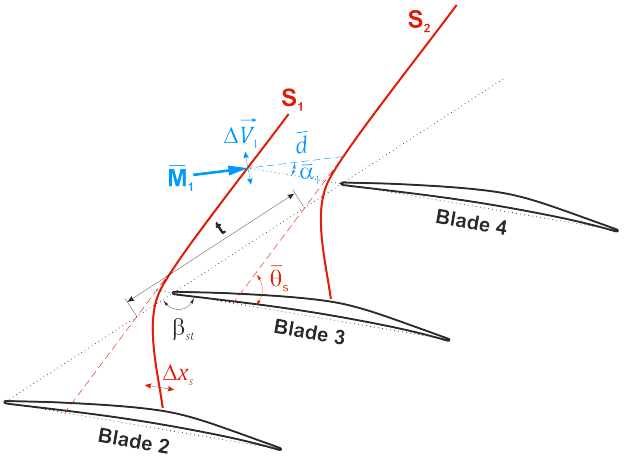

FIGURE 13: SIMPLIFIED SHOCK STRUCTURE AND PROPAGATION ANALYSIS BETWEEN BLADES 2 AND 3.

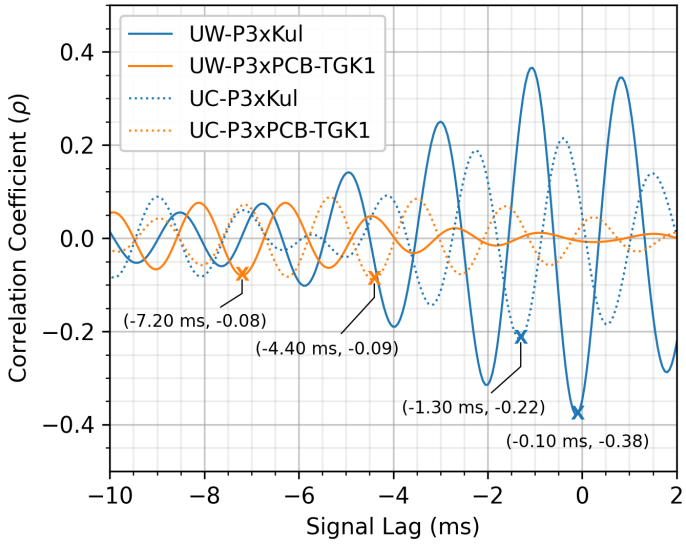

FIGURE 14: SHOCK POSITION SIGNAL CORRELATIONS BETWEEN THE CASCADE'S MIDDLE PASSAGE AND DOWNSTREAM UNSTEADY SENSORS

is some information traveling downstream between the passages with said time delay. In order to shed some light on these results, a geometrical analysis was performed based on a simplified and periodic shock structure, as shown in Fig. 13. The steady values are accentuated with a bar, while the disturbances are denoted with the symbol, Δ. Extending the main bow shock line reveals the angle with respect to the blade chord, $\overline{\theta}_S$. This angle can be reasonably approximated to 60°, based on the Schlieren (not time-resolved) images captured of the bow shocks, see Fig. 4.

Based on this analysis and the average inflow conditions measured noted in Tab. 1, it follows that the estimated average distance between the bow shocks ($\overline{d}$) is 23.3 mm, and the corresponding lag based on flow convection is approximately 0.062 ms. The propagation based on the flow speed and the speed of sound is also considered, providing an estimated lag of 0.034 ms. The measured lag of 0.050 ms then seems to lie in between these two estimates. Although it is hard to distinguish the main mechanism due to the nature of the unsteadiness, the results indicate that the events occurring in the lower passages readily propagate to the rest of the cascade. This, regardless of the nature of the disturbances, which may be due to the SBLI within the passages themselves or due to the possible interactions with the lower wind tunnel configuration. Noting that this half Laval nozzle is a common configuration for linear cascades [21], these observations may also apply to similar facilities. Lastly, an average estimated frequency of 535 Hz between correlation peaks may suggest that the main disturbances propagated are not related to the other frequencies measured in the wind tunnel, even though it still lies close to the 586 Hz frequency from the wind tunnel sidewall.

The correlation between the 3rd and 4th passages on the other hand is more difficult to interpret. For this set of results, it was generally found that the correlation has a very small value at zero lag, sometimes being closer to a trough than a peak. This suggests that the shocks are oscillating out of phase with one another and sometimes even in opposite directions. Additionally, the frequency between the peaks was 522 Hz and the highest-amplitude peak/trough always lied at a positive lag between 0.45 and 2.45 ms. As an exercise, the correlations between the 2nd and 4th passages were also performed and yielded similar results, as could have been expected. Although it might be tempting to state that the upper passage may also have an influence on the lower passages, the correlation results are not as consistent and the mechanism of any such influence would not be as obvious. It is clear however that the influence of the lower passages previously observed diminishes as the influence of the upper configuration of the wind tunnel becomes more relevant.

A similar procedure was performed with the other signals available, as shown in Fig. 14. In this figure, the 3rd passage has been correlated with the downstream Kulite and the PCB-TGK1 sensors with the same bypass filter between 400 and 700 Hz and annotated maxima. The results from the Kulite show that the signals correlate strongly at negative lags. These maxima have also been confirmed to be a factor of 4-5 times larger than other peaks in a reasonably large lag interval (-20 and 20 ms). This may indicate that there is a transmission of information in the downstream direction from the cascade to the Kulite, though the lag of the maxima is not consistent and was observed to vary between -0.1 and -1.2 ms. On the other hand, a simplified analysis of transmission based on the average outlet flow velocities previously measured estimates a lag of approximately -0.4 ms.

Finally, the correlations between the middle passage and the TGK1 sensor are also shown. Although the maxima are located still further downstream as could be expected, their values are comparable to other peaks in the -20 to 20 ms lag interval. Extracting any sort of information is then still more difficult, especially due to all the external influences that affect the flow as it travels further downstream of the probe. It is however still an interesting comparison and shows that all the signals are correlating with peak frequencies around 540 Hz. It also seems to indicate that there are signs of mostly downstream transmission from these signals instead of upstream transmission as could be theorized if the configuration of the wind tunnel was affecting the

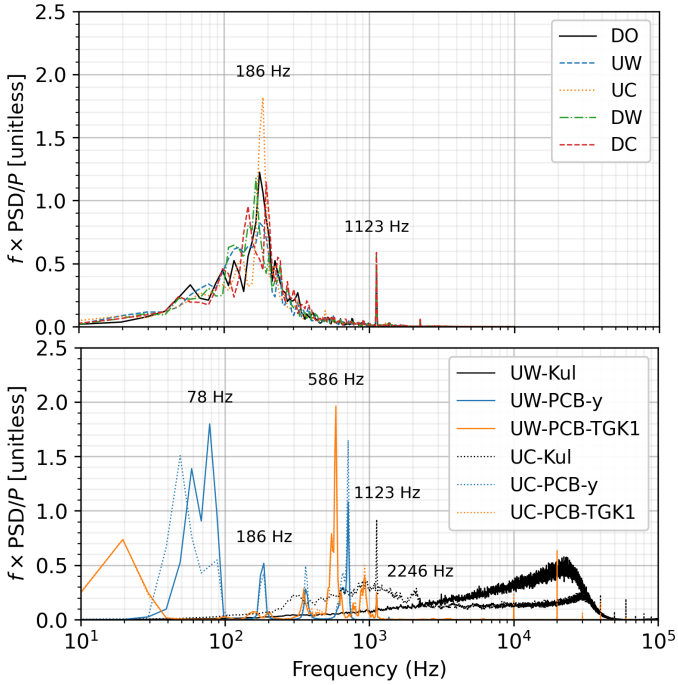

FIGURE 15: SHOCK POSITION FROM THE 3rd PASSAGE (TOP) AND KULITE, PCB-Y, AND PCB-TGK1 SENSOR (BOTTOM) SPECTRA OVER DIFFERENT PROBE POSITIONS AT THE CASCADE'S ODP

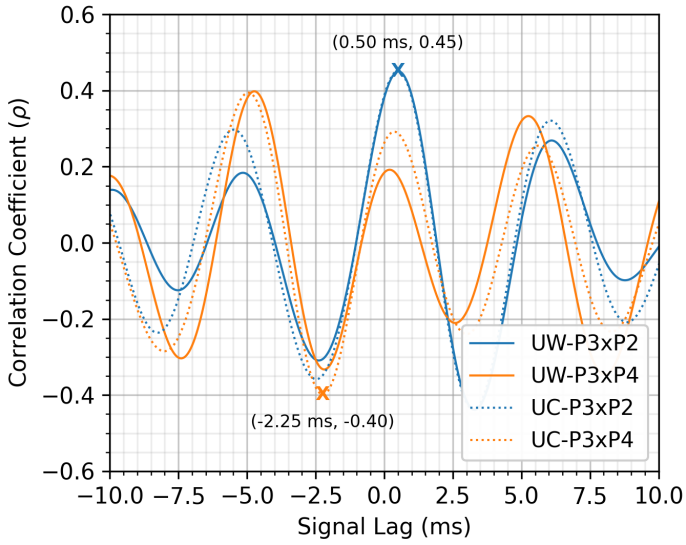

FIGURE 16: SHOCK POSITION SIGNAL CORRELATIONS BETWEEN THE CASCADE PASSAGES FOR THE UPWAKE AND UPCENTER POSITIONS

SBLI in the cascade passages. Further analyses were attempted with different filters near the 1.14 kHz tone, but they did not provide a lot of new information, given that the correlation maxima were always very similar in magnitude.

4.3 ODP: Analysis of the Unsteady Measurements

The measurements made at the ODP were also analyzed thoroughly and are presented in a brief manner. For this case, the shock structure was less periodic and it is reflected with average shock positions along the chord of 49.4%, 38.0%, and 35.5% for the 2nd, 3rd, and 4th passages, respectively. Even though the cascade is operating at a lower inlet Mach number, and therefore with at a smaller wake and losses, the range of the excursions are consistently high for the different passages with excursion ranges between 15% and 20% chord length. The PCB sensors on the other hand are generally moving at similar levels as before.

4.3.1 ODP: Signal Spectra Analysis. For these operating conditions, the spectra of the different passages were very similar to each other. Because of this, only the spectra of the shock position in the 3rd passage over the different measurement positions are shown in Fig. 15, along with the spectra from the Kulite, PCB-y, and TGK1 sensors. In the figure of the middle passage, the topology of the spectra is shown to be similar between the different probe positions. In addition to this, the main lower frequency band of the shock has clearly shifted to even lower frequencies between 100 and 300 Hz, with the peak now located at 186 Hz. The high frequency tone is also present, albeit with a slightly lower frequency of 1123 Hz. Although the change of inlet Mach number reduced both the main broadband frequency band and the tone previously noted for the cascade's ADP, it is clear that the frequency shift has disproportionately affected the lower frequency band and that the high-frequency tone remains largely unaffected in comparison.

The spectra of the other unsteady sensors on the other hand has stayed very similar, if not identical, to the ones shown for the ADP. The Kulite spectra for instance shows a generally broadband spectrum up to frequencies in the order of 10^4. The lower frequency band from the passage is once again not visible, unlike the high frequency tone and its first harmonic, now at 2246 Hz. The Kulite, just like before, is also showing higher energy content at high frequencies in the Wake MP compared to the Center one. The PCB sensors on the other hand show almost identical spectra as before. Notably, the sidewall is still vibrating mainly at a frequency band between 500 and 600 Hz, with a peak at 586 Hz. For this operating point, it is then evident that the movement of the sidewall, at the TGK1 sensor at least, is completely decoupled from the main movement of the shocks within the cascade passages.

4.3.2 ODP: Signal Correlations. One last correlation analysis between the cascade passages is shown in Fig. 16. For these analyses, the signal has been bypass filtered again to the relevant frequencies, this time estimated to be between 100 and 300 Hz. Once again, the lines shown for the UpWake and UpCenter positions are representative of what was observed with other possible combinations. In this case, the correlations show one more time that the 3rd and 2nd passages correlate strongly at a peak, with a downstream transmission of information between the passages. The lag between these passages is also again very consistent across recordings and measurement positions, showing a delay of 0.50 ms. This time however, a simplified analysis of the shock structure with average inflow conditions provides a lag estimate of 0.26 ms, about a half of the one obtained with the correlations. This may be due to the more aperiodic shock structure, which

makes it harder to estimate on average any possible downstream path of transmission. It could also however indicate that there is a different mechanism of transmission between the shocks at play, or simply other influences on the entire shock structure that haven't been considered yet and that also propagate downstream.

Lastly, the 3rd and 4th passages are notably shown this time to correlate more strongly with a negative lag, indicating that there is a downstream transmission between these passages as well. This, although it is not clear whether the correlation is at a maximum at the -2.25 ms trough, or at the -4.80 ms peak. The passages are however this time shown to be moving in-phase with each other, marking another difference with respect to the behavior observed at ADP operating conditions. Lastly, the correlations showed on average a lag between peaks of 168.8 Hz, on par with the observations made from the spectra in Fig. 15.

5. CONCLUSIONS AND PERSPECTIVES

In this paper, the SBLI of a modern transonic compressor cascade has been studied in detail at the ADP and at an ODP. Measurements of the interaction were performed employing a unique set of experimental methods, including simultaneous unsteady measurements of the shock position in three adjacent cascade passages, of the total pressure at the cascade outlet, and of the movement of the probe and wind tunnel sidewalls.

The analysis of the data showed that the movement of the shock had a similar topology for both operating points. Namely, the SBLI showed a main shock oscillation at a lower broad frequency band in the order of 10^2 Hz and a distinct tone over 1000 Hz. However, the frequencies in question were distinctly different between the operating points, with the ADP showing frequencies peaking near 520-550 Hz, and the ODP showing much lower frequencies around 180 Hz. The spectra of the different wind tunnel components on the other hand showed consistent frequencies across operating points. The TGK's sidewall for example showed a dominant frequency peak at 586 Hz for both operating conditions, even when the shock was oscillating with similar frequencies for the cascade's ADP. This suggests that the movement of the sidewall is not related to the frequencies being observed and measured in the passages.

These results help shed some light on the complex interactions that occur within a transonic cascade of the kind, first due to the SBLI itself, but second possibly also due to the complex configurations of the facilities required to operate them. From correlating the different signals, all the influences that could be possibly acting on the cascade based on the unique data gathered were investigated. From this exercise, it was generally established that the 2nd and 3rd cascade passages are closely linked to each other based on the conditions of the incoming flow. Additionally, there may be at least one more possible mechanism of interaction between these passages, causing a delayed flow of information downstream for some operating points. The 4th passage on the other hand seems to show a shock behavior that is distinctly different from the other two throughout. This indicates that there are still other mechanisms present that influence the operation of the cascade in the upstream direction.

All in all, the data presented is a good start towards understanding the numerous and complex SBLI mechanisms within the wind tunnel. This information will certainly help plan and prepare future studies at the TGK with the aim of thoroughly understanding these mechanisms down the line. Further improvements include, for example, the installation of more unsteady sensors at new positions of interest, such as the upper and lower tailboards of the wind tunnel; or adding more measurement techniques, such as PIV and High-Speed PIV, with targeted configurations to complement the information that is gathered with the HSS visualization. Finally, the data gathered will also aid the planning and preparation of future efforts with high-fidelity CFD methods. A targeted use of these methods to complement the unsteady experimental data could help unlock many of the questions that are still present regarding these interactions. One such CFD project is already underway in the department with the TCTA cascade under the framework of the TEAMAero consortium mentioned.

Regardless of whether the SBLI frequencies measured inside the wind tunnel are partly influenced by the facility itself or not, it is clear that the institute is making significant steps towards identifying these mechanisms. These efforts meaningfully inform future research on the topic, whether numerical or experimental, to advance the knowledge base for the research community.

ACKNOWLEDGMENTS

This project has received funding from the European Union's Horizon 2020 research and innovation programme under grant agreement No EC grant 860909. The authors would also like to thank the continued support from the different DLR departments involved in obtaining and analyzing this unique set of data, which has helped bring unique knowledge and expertise to the institute.

REFERENCES

[1] Dolling, D. S. "Fifty years of shock-wave/boundary-layer interaction research: What next?" *AIAA Journal* Vol. 39 No. 8 (2001). DOI 10.2514/2.1476.

[2] Lee, B. H.K. "Oscillatory shock motion caused by transonic shock boundary-layer interaction." *AIAA Journal* (1990)DOI 10.2514/3.25144.

[3] Lee, B. H.K. "Self-sustained shock oscillations on airfoils at transonic speeds." (2001). DOI 10.1016/S0376-0421(01)00003-3.

[4] Crouch, Jeffrey D., Garbaruk, A., Magidov, D. and Travin, A. "Origin of transonic buffet on aerofoils." *Journal of Fluid Mechanics* (2009)DOI 10.1017/S0022112009006673.

[5] Hergt, Alexander, Klinner, Joachim, Willert, Christian, Grund, Sebastian and Steinert, W. "Insights into the Unsteady Shock Boundary Layer Interaction." *Turbo Expo: Turbomachinery Technical Conference and Exposition (GT2022)*. 2022. American Society of Mechanical Engineers, Rotterdam. DOI 10.1115/GT2022-82720.

[6] Klinner, Joachim, Hergt, Alexander, Grund, Sebastian and Willert, Christian E. "High-Speed PIV of shock boundary layer interactions in the transonic buffet flow of a compressor cascade." *Experiments in Fluids* Vol. 62 No. 3 (2021). DOI 10.1007/s00348-021-03145-3.

[7] Dupont, P., Piponniau, S., Sidorenko, A. and Debiève, J. F. "Investigation by particle image velocimetry measurements

of oblique shock reflection with separation." *AIAA Journal* Vol. 46 No. 6 (2008). DOI 10.2514/1.30154.

[8] Beresh, S. J., Clemens, N. T. and Dolling, D. S. "Relationship between upstream turbulent boundary-layer velocity fluctuations and separation shock unsteadiness." *AIAA Journal* Vol. 40 No. 12 (2002). DOI 10.2514/2.1609.

[9] Touber, Emile and Sandham, Neil D. "Large-eddy simulation of low-frequency unsteadiness in a turbulent shock-induced separation bubble." *Theoretical and Computational Fluid Dynamics* Vol. 23 No. 2 (2009). DOI 10.1007/s00162-009-0103-z.

[10] Garnier, E. and Deck, S. "Large-eddy simulation of transonic buffet over a supercritical airfoil." *Notes on Numerical Fluid Mechanics and Multidisciplinary Design*. 2010. DOI 10.1007/978-3-642-14139-3-16.

[11] Priebe, Stephan, Wilkin II, Daniel, Breeze-Stringfellow, Andy, Mousavi, Arash, Bhaskaran, Rathakrishnan and D'Aquila, Luke. "Large Eddy Simulations of a Transonic Airfoil Cascade." (2022). DOI 10.1115/GT2022-80683. URL https://doi.org/10.1115/GT2022-80683.

[12] Hergt, Alexander, Klinner, J., Wellner, J., Willert, C., Grund, S., Steinert, W. and Beversdorff, M. "The Present Challenge of Transonic Compressor Blade Design." *Journal of Turbomachinery* (2019)DOI 10.1115/1.4043329.

[13] Epstein, A. H., Kerrebrock, J. L. and Thompkins, W. T. "Shock structure in transonic compressor rotors." *AIAA Journal* Vol. 17 No. 4 (1979). DOI 10.2514/3.61134.

[14] Hah, C. and Reid, L. "A viscous flow study of shock-boundary layer interaction, radial transport, and wake development in a transonic compressor." *Journal of Turbomachinery* Vol. 114 No. 3 (1992). DOI 10.1115/1.2929177.

[15] Doerffer, Piotr, Hirsch, Charles, Dussauge, J.-P, Babinsky, Holger and Barakos, George. *Unsteady Effects of Shock Wave Induced Separation*. Vol. 114 (2011). DOI 10.1007/978-3-642-03004-8.

[16] Doerffer, Piotr, Flaszynski, Pawel, Dussauge, J.-P, Babinsky, Holger, Grothe, Patrick, Petersen, Anna and Billard, Flavien. *Transition Location Effect on Shock Wave Boundary Layer Interaction Experimental and Numerical Findings from the TFAST Project: Experimental and Numerical Findings from the TFAST Project* (2021). DOI 10.1007/978-3-030-47461-4.

[17] Hartmann, A., Feldhusen, A. and Schröder, W. "On the interaction of shock waves and sound waves in transonic buffet flow." *Physics of Fluids* (2013)DOI 10.1063/1.4791603.

[18] Berto, Federico, Benini, Ernesto, Wyatt, Ciaras and Quinn, Mark Kenneth. "Time-accurate experimental investigation of hypersonic inlet buzz at Mach 5." *AIAA Journal* Vol. 58 No. 5 (2020). DOI 10.2514/1.J058764.

[19] Schreiber, H-A and Starken, H. "Evaluation of blade element performance of compressor rotor blade cascades in transonic and low supersonic flow range." *International Symposium on Air Breathing Engines, 5 th, Bangalore, India*: pp. 61–67. 1981.

[20] Schreiber, H A and Starken, H. "On the definition of the axial velocity density ratio in theoretical and experimental cascade investigations." *Measuring techniques in transonic and supersonic flows in cascades and turbomachines* (1982): pp. 1–7.

[21] Hirsch, Charles. "Advanced Methods for Cascade Testing." *AGARDOgraph* Vol. AGARD-AG-3 (1993): pp. 35–59.

[22] Munoz Lopez, Edwin Joseph, Hergt, Alexander and Grund, Sebastian. "The New Chapter of Transonic Compressor Cascade Design at the DLR." *Volume 1: Aircraft Engine; Ceramics and Ceramic Composites*, Vol. 1: p. V001T01A005. 2022. American Society of Mechanical Engineers, Rotterdam. DOI 10.1115/GT2022-80189. URL https://asmedigitalcollection.asme.org/GT/proceedings/GT2022/85970/V001T01A005/1148590.

[23] Munoz Lopez, Edwin Joseph, Hergt, Alexander, Grund, Sebastian and Gümmer, Volker. "The New Chapter of Transonic Compressor Cascade Design at the DLR." *Journal of Turbomachinery* (2023): pp. 1–23DOI 10.1115/1.4056982. URL https://doi.org/10.1115/1.4056982.

[24] TEAMAero. "Towards Effective Flow Control and Mitigation of Shock Effects in Aeronautical Applications (TEAMAero)." (2021). Accessed 2020-12-03, URL https://h2020-teamaero.eu.

[25] Voß, Christian, Aulich, Marcel, Kaplan, Burak and Nicke, Eberhard. "Automated multiobjective optimisation in axial compressor blade design." *Proceedings of the ASME Turbo Expo*, Vol. 6 PART B. 2006. Barcelona. DOI 10.1115/GT2006-90420.

[26] Becker, Kai, Heitkamp, Kathrin and Kuegeler, Edmund. *Recent Progress In A Hybrid-Grid CFD Solver For Turbomachinery Flows* (2010).

[27] Schodl, R. "Laser Dual-Beam Method for Flow Measurements in Turbomachines." *American Society of Mechanical Engineers (Paper)*. 74 -GT-157. 1974.

[28] Hurst, Adam M., Olsen, Timothy R., Goodman, Scott, VanDeWeert, Joe and Shang, Tonghuo. "An experimental frequency response characterization of MEMS piezoresistive pressure transducers." *Proceedings of the ASME Turbo Expo*, Vol. 6. 2014. DOI 10.1115/GT2014-27159.

[29] Willert, C., Stasicki, B., Klinner, J. and Moessner, S. "Pulsed operation of high-power light emitting diodes for imaging flow velocimetry." *Measurement Science and Technology* (2010)DOI 10.1088/0957-0233/21/7/075402.

[30] Willert, Christian, Mitchell, Daniel Michael and Soria, Julio. "An assessment of high-power light-emitting diodes for high frame rate schlieren imaging." (2012). DOI 10.1007/s00348-012-1297-1. URL http://link.springer.com/article/10.1007{%}2Fs00348-012-1297-1.

[31] Klinner, Joachim, Schroll, Michael, Lengyel-Kampmann, Timea, Belz, Joachim, Eichner, Franziska, Winkelmann, Peter and Willert, Christian. "Measurement of Aerodynamically Induced Blade Distortion on a Shrouded Counter-Rotating Prop-Fan." *20th International Symposium on Application of Laser and Imaging Techniques to Fluid Mechanics*. 2022. URL https://www.lisbonsimposia.org/.